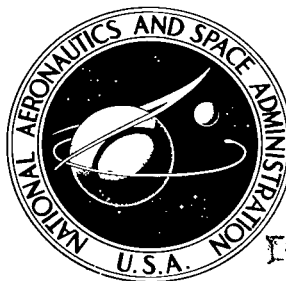
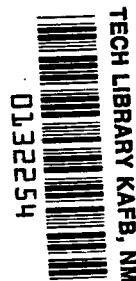


NASA TECHNICAL NOTE



NASA TN D-5274

NASA TN D-5274



A LABORATORY STUDY OF
MICROWAVE RADIOMETRIC TECHNIQUES
FOR RE-ENTRY PLASMA MEASUREMENTS

by P. R. Caron, G. Haroules, W. Brown III, and F. Russo

*Electronics Research Center
Cambridge, Mass.*



A LABORATORY STUDY
OF MICROWAVE RADIOMETRIC TECHNIQUES
FOR RE-ENTRY PLASMA MEASUREMENTS

By P. R. Caron, G. Haroules, W. Brown III, and F. Russo

Electronics Research Center
Cambridge, Mass.

NATIONAL AERONAUTICS AND SPACE ADMINISTRATION

For sale by the Clearinghouse for Federal Scientific and Technical Information
Springfield, Virginia 22151 - CFSTI price \$3.00

A LABORATORY STUDY OF MICROWAVE RADIOMETRIC TECHNIQUES FOR RE-ENTRY PLASMA MEASUREMENTS

By P. R. Caron, G. Haroules, W. Brown, III, and F. Russo
Electronics Research Center

SUMMARY

The results of a laboratory study of plasma radiometric techniques applicable to reentry plasma measurements are presented. The laboratory plasma is generated by a glow discharge in helium using a large V-groove cathode. The operating characteristics of the discharge are quite similar to those of the brush cathode discharge. The electron density and temperature are determined as a function of position, discharge current, and gas pressure using Langmuir probes and microwave reflectometers, and the collision frequency is calculated using these measured values. The plasma noise radiation is measured as a function of discharge current using a microwave radiometer operating in the absolute mode and it is shown that numerical values of electron density, collision frequency and electron temperature can be derived from curves of plasma noise as a function of discharge current. For the negative glow discharge used in this study the collision frequency and the temperature are relatively low and are difficult to determine independently and accurately. For the re-entry plasma associated with large, high-speed vehicles, on the other hand, they are relatively high and can both be obtained with reasonable accuracy. In this case however, it is necessary to measure plasma noise as a function of frequency, which requires a swept-frequency radiometer or several fixed frequency devices.

I. INTRODUCTION

There is a need for diagnostic techniques and devices for measuring the characteristic parameters of re-entry plasmas. Three of the important parameters of these plasmas are the electron density, the electron temperature, and the total electron collision frequency. These parameters are determined by the aerodynamic characteristics, the speed, and the altitude of the re-entry vehicle. For a wide class of vehicles and missions, the re-entry plasmas cause degradation in the communication signal from and to the vehicle to the extent that complete blackout of the signal exists for a time duration which, in general, increases with the size and speed of the vehicle.

A substantial amount of predicted data exists for the plasma parameters and resulting electromagnetic attenuation of a wide variety of vehicles and missions. However, reliable measurements of the plasma parameters are scarce, and comparisons between these

data and the predicted values have only been accomplished with good agreement in a limited number of cases. Among the most notable programs where a serious attempt has been made to measure and understand re-entry plasmas are the RAM vehicle program and the Trailblazer program. In these programs, many types of plasma diagnostic devices were used, one of which was a microwave radiometer to measure plasma noise. The experiment was not successful on the RAM vehicles, but the Trailblazer temperatures were measured successfully. (ref. 1). Microwave radiometers have been used extensively in the laboratory for measuring electron temperatures. For more details the reader is referred to Bekefi (ref. 2) and to the references given in his book. The technique most often used is to insert the plasma in a waveguide and compare the noise power of the plasma with that from the combination of a standard noise tube and a variable attenuator. With a variation of this technique, Ingraham (ref. 3) showed that the plasma temperature can be obtained independently of the plasma reflection coefficient and the magnitude of the plasma attenuation. Clearly, this technique cannot be fully implemented in a re-entry experiment. Caldecott (ref. 1) compensated for the effect of plasma reflections by measuring the power reflection coefficient using an incoherent source, but he assumed a large plasma attenuation. In this report, no attempt will be made to eliminate the effects of either the reflection coefficient or the absorption length, but these phenomena will be utilized for diagnostic purposes. It will be shown that, in this case, it is possible to obtain not only the electron temperature but the electron density and the collision frequency.

II. THE COLD CATHODE DISCHARGE

The plasma is generated by a cold-cathode, abnormal glow discharge in helium. The discharge configuration is shown in Figure 1. For the radiometer measurements, it is advantageous to make the anode-to-cathode distance, d , small compared to the tube diameter in order to minimize the effects of radial electron density profiles. Hence, d is chosen to be half the tube diameter which is 12 inches. The cathode is a 12-inch diameter aluminum plate with milled V-grooves of 60 deg angle and 1/8 inch-spacing. With these grooves, the cathode current caused by secondary emission processes (e.g., ion-bombardment and photoelectric emission) remains uniform over the cathode surface in the abnormal glow region; that is, the tendency for a localized discharge or arc to form is reduced. Such formations generally appear in large, flat cathodes. Also, the grooves increase the effective cathode area and increase the electron yield by ion-bombardment caused by oblique incidence of ions on the cathode (ref. 4).

The chamber is pumped down to low pressure and backfilled with helium. To improve the gas purity, helium is allowed to flow

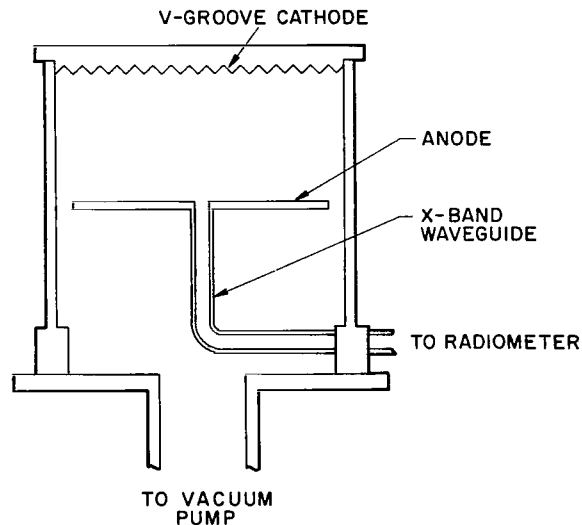


Figure 1. - Sketch of the V-groove cathode discharge configuration

continuously through the chamber at a slow rate, and the pressure is adjusted by means of a leak valve in series with the helium supply. A dc voltage applied between the anode and cathode produces a negative glow discharge, the behavior of which is qualitatively similar to that of a brush cathode discharge (ref. 5); that is, the plasma is beam-generated and the electron density is sufficiently high (i.e., on the order of 10^{12} e/cm³) and the electron temperature is sufficiently low (i.e., approximately 1200°K) so that electron-ion recombination* is the dominant electron-loss mechanism.

The voltage-current characteristic in the abnormal glow region is shown in Figure 2 for various pressures. At low currents, there is a negative resistance phenomenon which is not displayed in these curves. These characteristics, as well as the plasma parameters, are dependent upon the purity of the helium and the condition of the cathode surface which, in turn, depend upon the discharge current and the helium flow rate. No attempt was made to obtain an ultraclean cathode since its size made this nearly impossible, and the purity of the discharge was not crucial to the objects of the experiment. However, the reproducibility of the results is important and was obtained by operating the discharge with the same helium flow rate at each pressure and only recording data at each current after the discharge had stabilized. This procedure yielded excellent data.

*This is most likely collisional-radiative recombination (ref. 6) with perhaps some disassociative recombination at the higher pressures of operation.

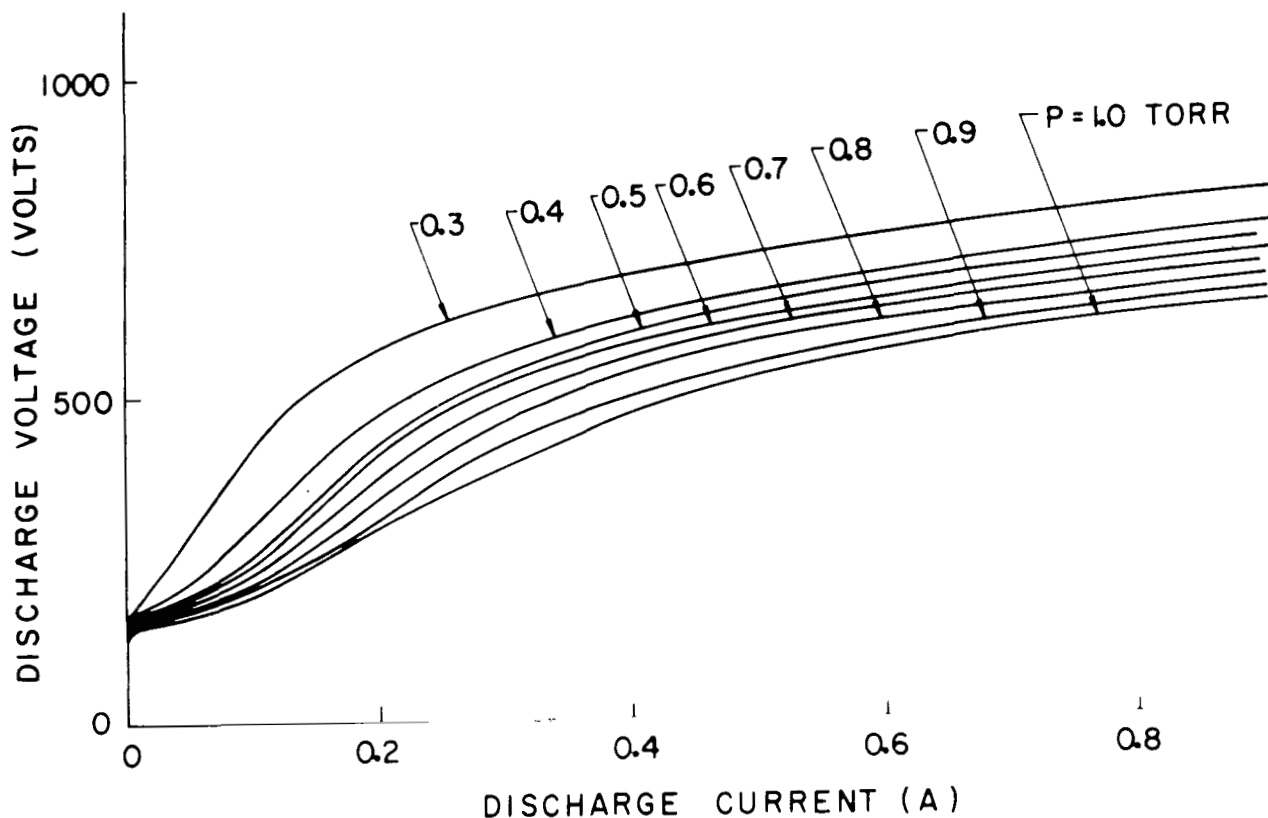


Figure 2. - Voltage-current characteristics of the V-groove cathode discharge

Figure 2 shows that the operating voltage for a given current is substantially lower than that of the brush cathode discharge developed by Persson (ref. 5). This is due to the higher secondary emission coefficients of aluminum compared to the coefficients for the materials used by Persson. Thus, not only is the V-groove cathode easier to fabricate,* but it also results in far less cathode dissipation for the same discharge current. Furthermore, the lower beam voltage results in a larger source function for electron-ion generation near the cathode, because the ionization mean free path is smaller at these lower beam voltages. Typically, the voltage results in beam energies yielding electron-ion source functions near the maximum value in helium. Also, the lower operating voltage tends to lessen the arcing which sometimes occurs

*This is of particular importance for this experiment since the cathode is so large.

near the glass container at the cathode. The disadvantage of the lower operating voltage is that the primary beam-reaching distance is smaller than that of the conventional brush cathode discharge. Since electron-ion recombination is the dominant electron loss mechanism, this results in a substantial decay in the secondary electron number density in the axial direction away from the cathode. This effect occurs for all discharge currents up to 900 mA at pressures above 0.8 torr and at sufficiently low voltages and currents for pressures below this value.

The visual appearance of the discharge at applied voltages comparable to the normal cathode fall voltage is a weak blue-green glow in the chamber. As the voltage is increased, the glow quickly changes to a deep pink color in the center of the discharge region and is surrounded by a blue-green boundary near the electrodes and the glass wall. The thickness of this boundary decreases with increasing pressure. The pink color is indicative of recombination in helium, and the blue-green boundary defines the region where the primary electron loss mechanism changes from volume recombination to ambipolar diffusion to the walls. For small operating voltages at the lower pressures (i.e., 0.4 to 0.8 torr), and for all operating voltages at higher pressures, the glow is most intense near the cathode. At high operating voltages and currents, and at pressures less than 0.8 torr, the discharge is visually symmetrical relative to the center of the chamber.

III. MEASUREMENTS OF THE PLASMA PARAMETERS

A movable Langmuir probe was used to obtain electron density and temperature as a function of position, discharge current, and gas pressure. For the range of parameters over which the discharge was operated, the electron temperature is constant. A typical set of Langmuir probe current-voltage curves at a fixed pressure (0.6 torr) and a fixed position (near the center of the discharge chamber) for discharge currents ranging from 0.1 to 0.9A is shown in Figure 3. (Since the saturation electron current can be determined quite accurately from these data and the electron temperature is constant, the reduction of these curves to semilog curves was not done in the bulk of the data reduction.) Figures 4 through 7 show electron density profiles in the axial direction for various pressures and discharge currents. The independent variable is normalized to 3 inches and the electron density is normalized to its peak value. The solid curves in these figures are theoretical profiles based on a diffusion-recombination model. Figures 8 through 14 show peak electron densities as a function of discharge currents for various pressures. The radial electron density profile was also obtained but is not considered pertinent to the results of this investigation.

Although previous investigations (ref.5) have shown Langmuir probe data to be of questionable accuracy in a beam-generated

plasma, no difficulty was encountered with the V-groove cathode except when the probe was placed quite near the cathode (i.e., within the blue-green boundary near this electrode). It is likely that the improvement is due to the lower operating voltage of the discharge, which gives a less energetic beam.

An X-band microwave reflectometer was connected to an open-ended waveguide port positioned in the center of the anode. The reflection coefficient of the open-ended guide plus plasma layer was monitored as a function of discharge current for fixed frequency and as a function of frequency for fixed discharge current. In either case, the transition from low to high reflection is well defined and determines quite accurately (ref. 7) the condition $\omega = \omega_p$ where ω_p is the plasma frequency and ω is the wave frequency of the reflectometer. Except for operating conditions in which there is a sizable beam decay, the plasma frequency corresponds to the peak electron density. The electron densities obtained by this method are compared with the peak densities measured by the probe in Figures 8 through 14. The agreement is consistent with the accuracies of the two measurement techniques.

There is no accurate method for measuring the collision frequency of a large, dense plasma. However, from knowledge of the electron temperature, the gas type and pressure, and the ion density, it is possible to calculate the collision frequency. At the relatively low electron temperature and high electron densities generated by the V-groove cathode discharge, electron-ion

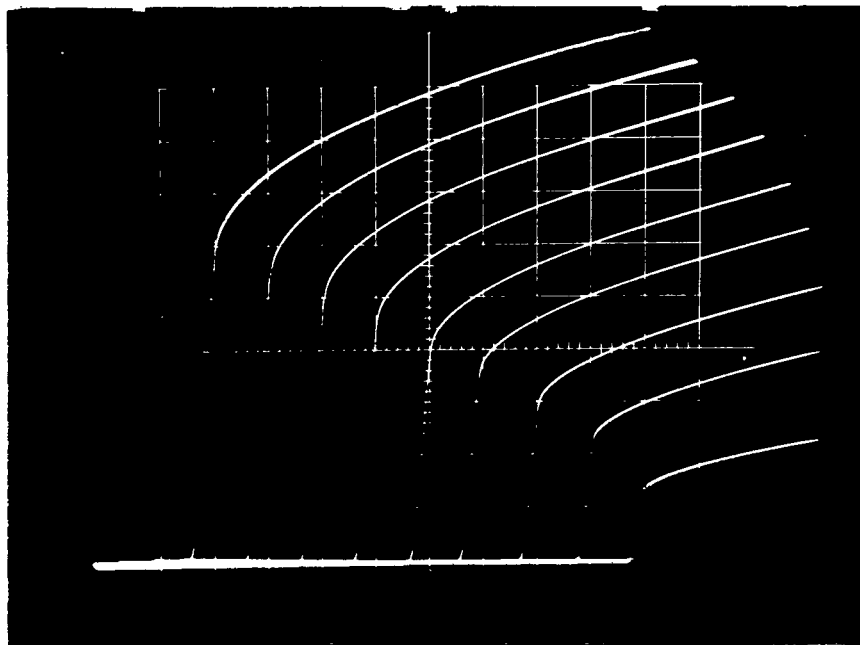
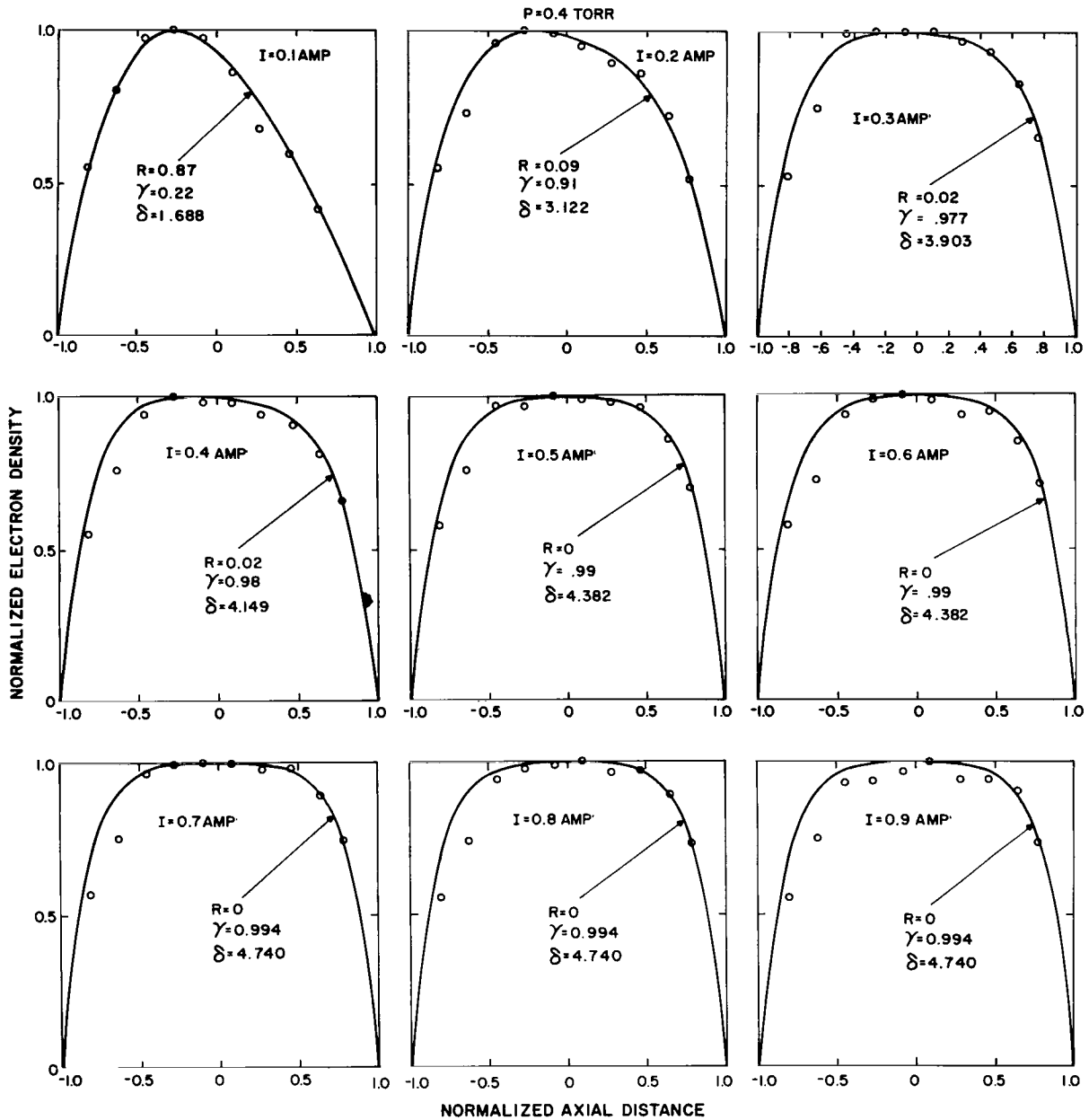


Figure 3. - Langmuir probe current-voltage curves for $p = 0.6$ torr and for discharge currents ranging from 0.1 to 0.9 A



ERC 5147

Figure 4. - Normalized electron density profiles as a function of normalized axial distance (cathode designated by -1 and anode by +1) for $p = 0.4$ torr

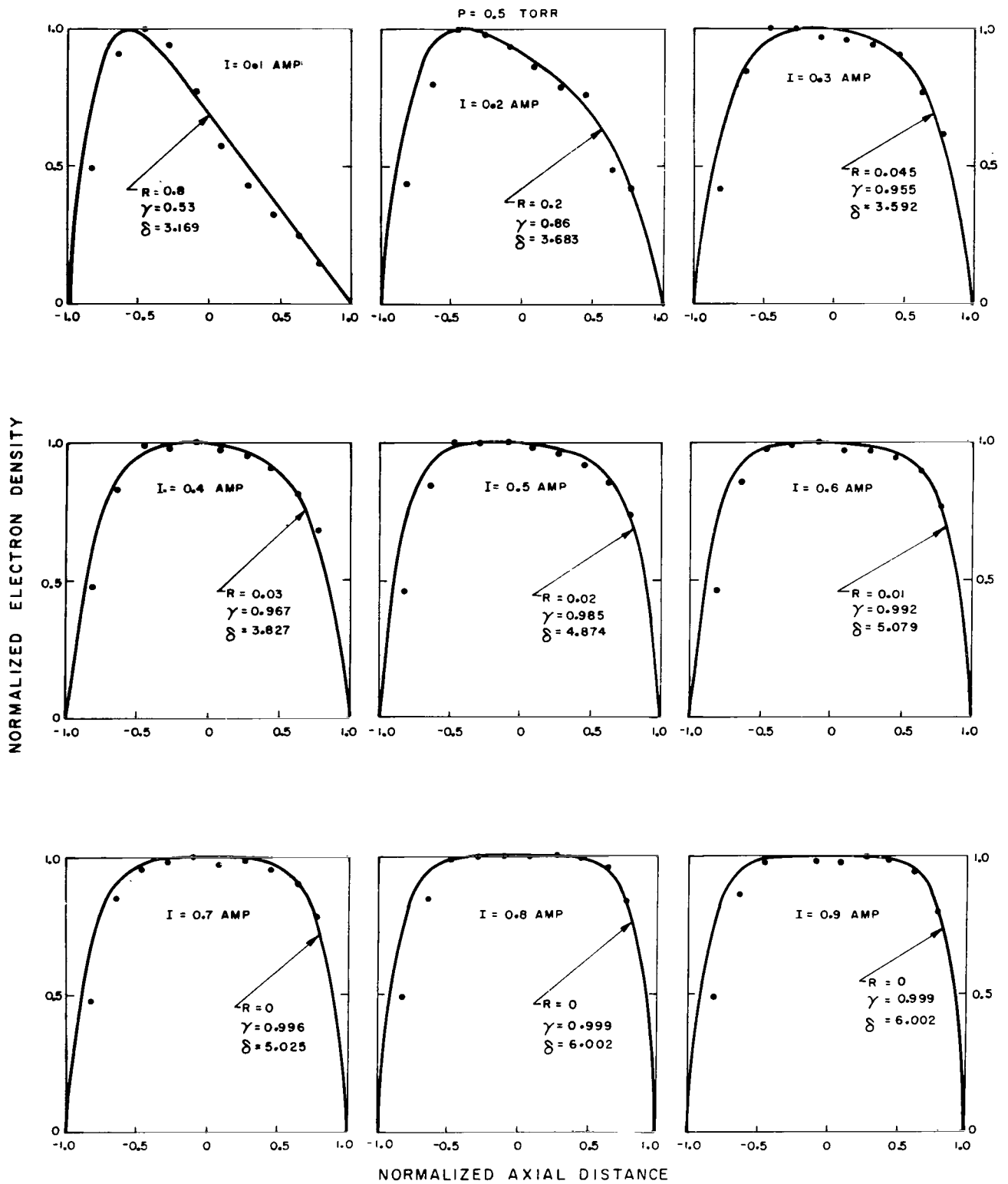


Figure 5. - Normalized electron density profiles as a function of normalized axial distance (cathode designation by -1 and anode by +1) for $p = 0.5$ torr

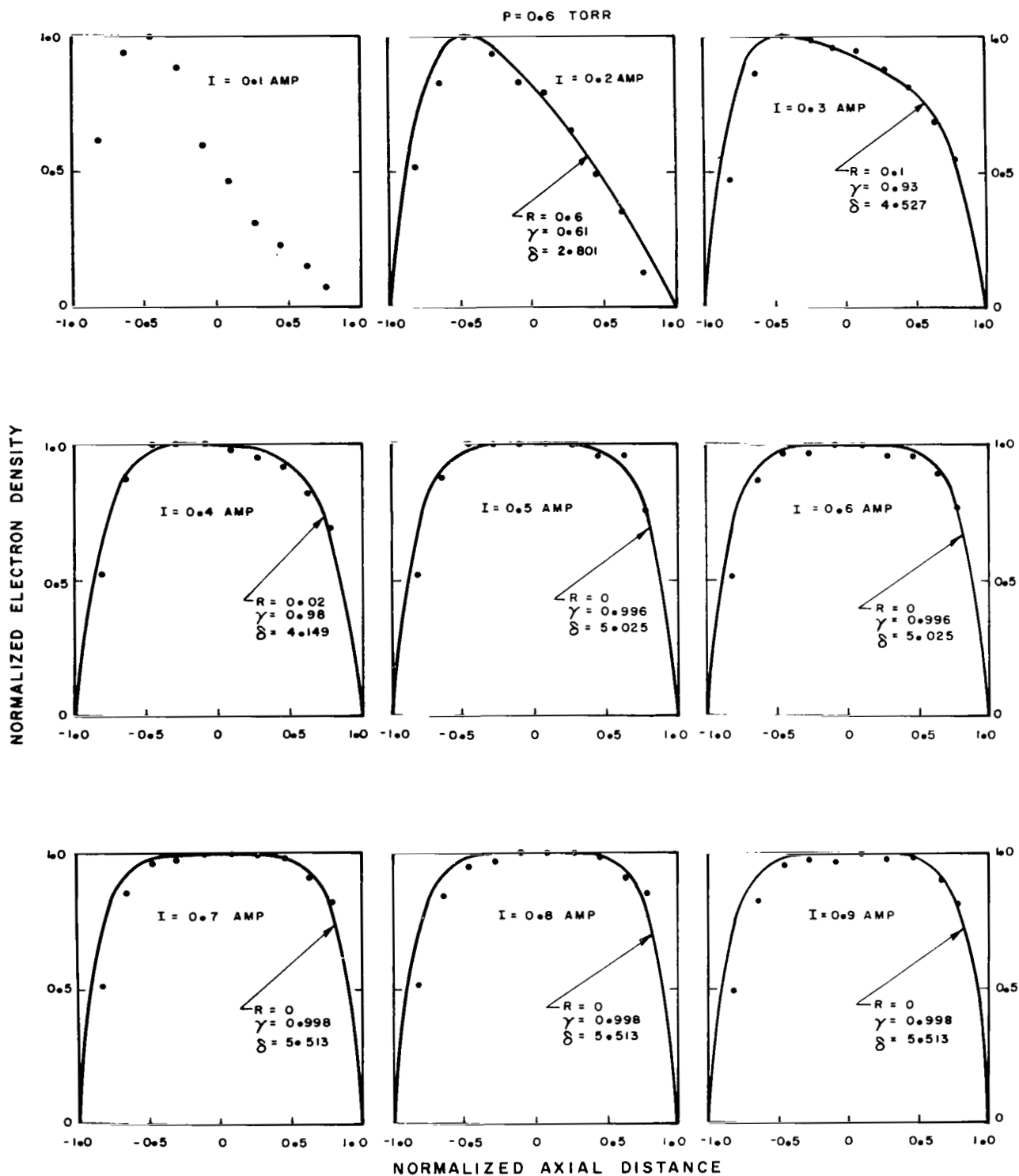


Figure 6. - Normalized electron density profiles as a function of normalized axial distance (cathode designated by -1 and anode by +1) for $p = 0.6$ torr

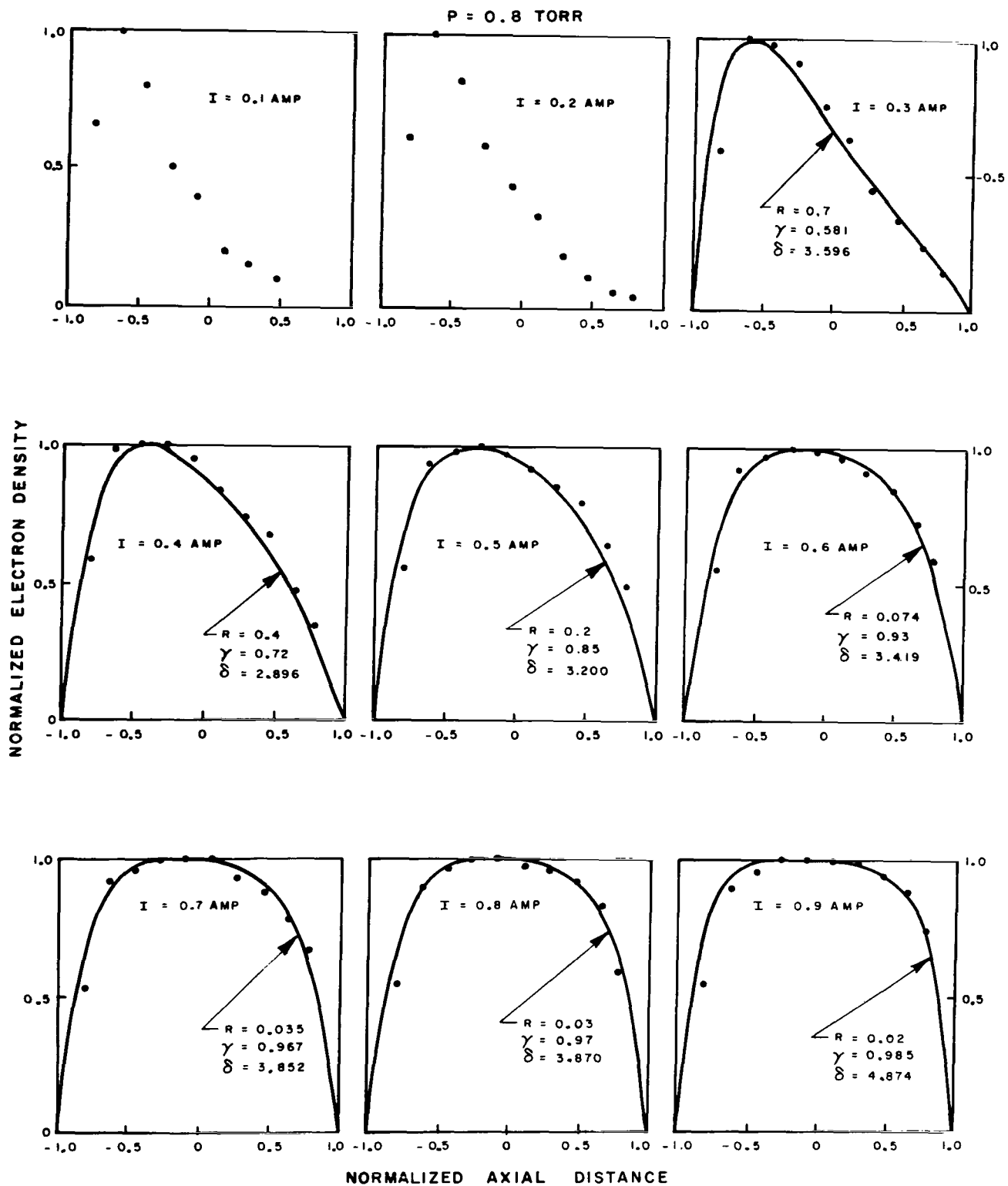


Figure 7. - Normalized electron density profiles as a function of normalized axial distance (cathode designated by -1 and anode by +1) for $p = 0.8$ torr

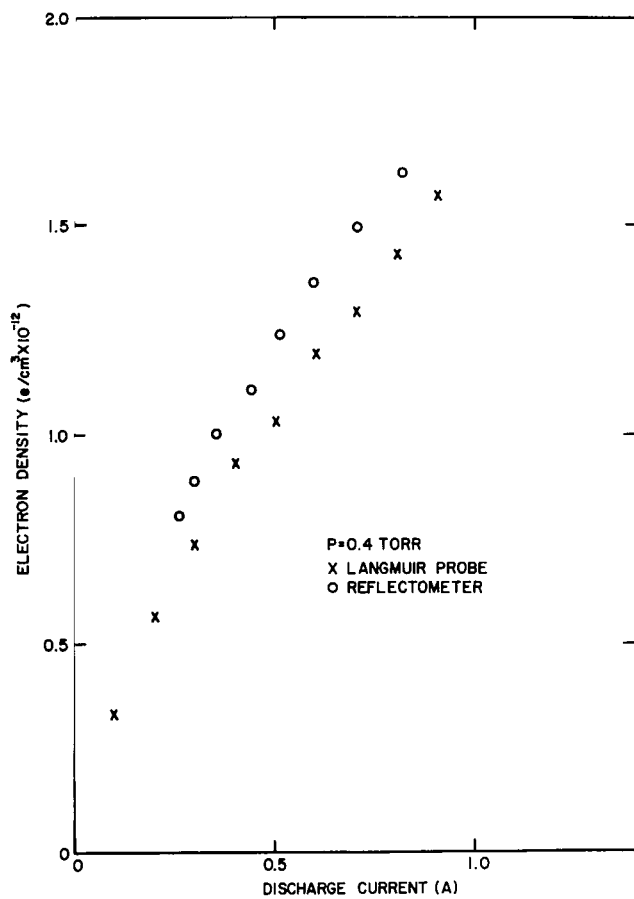


Figure 8.- Peak electron density as a function of discharge current for $p = 0.4$ torr

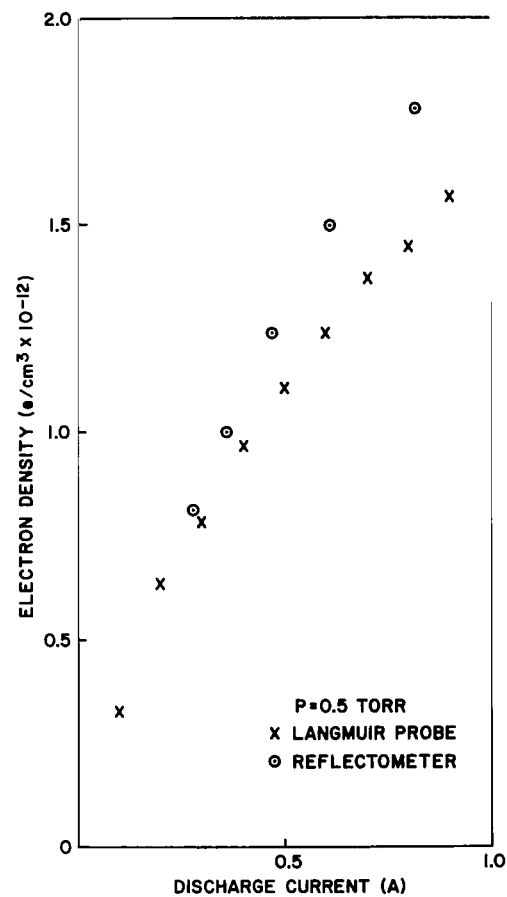


Figure 9.- Peak electron density as a function of discharge current for $p = 0.5$ torr

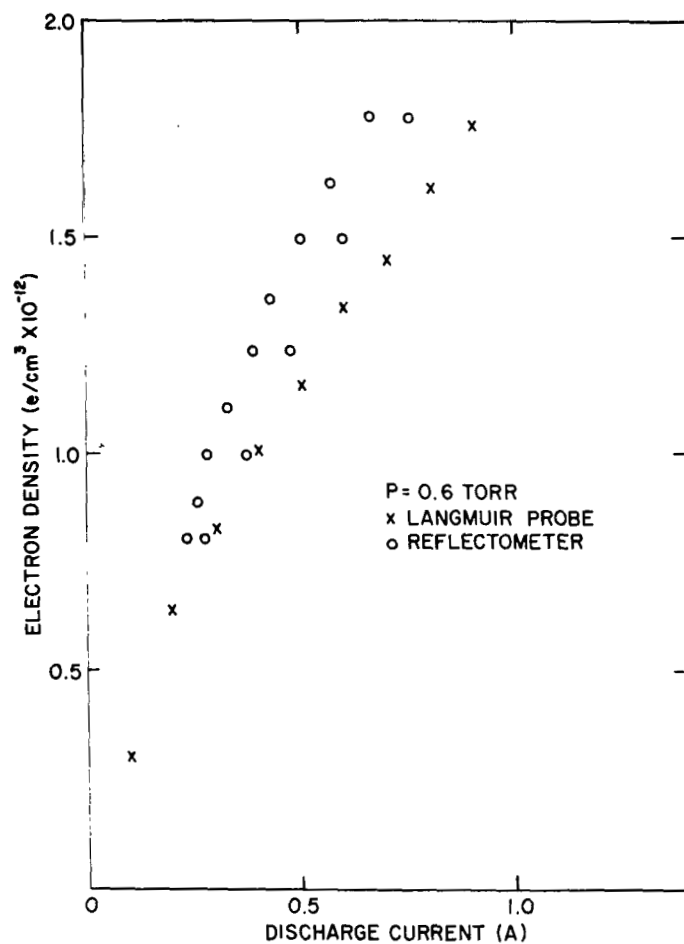


Figure 10.- Peak electron density as a function of discharge current for $p = 0.6$ torr

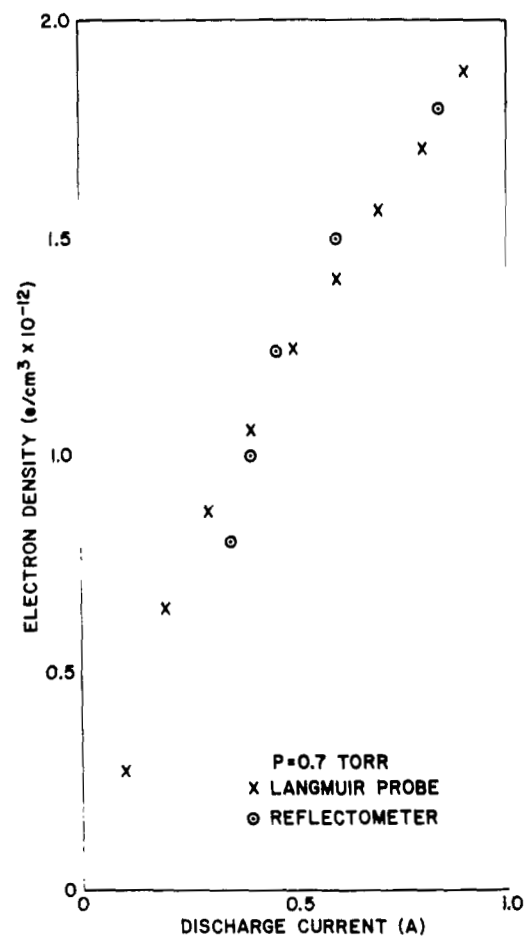


Figure 11.- Peak electron density as a function of discharge current for $p = 0.7$ torr

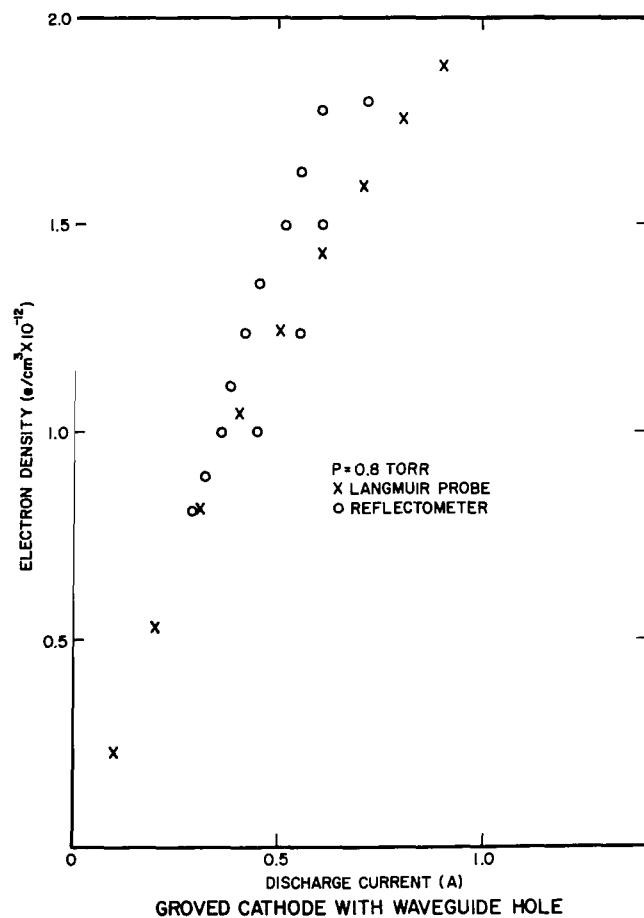


Figure 12.- Peak electron density as a function of discharge current for $p = 0.8$ torr

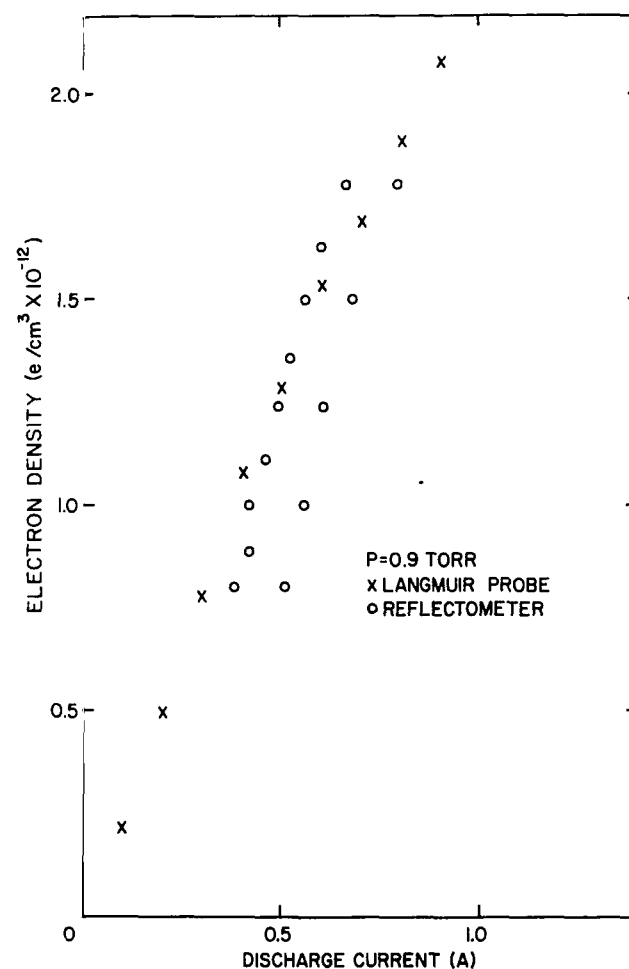


Figure 13.- Peak electron density as a function of discharge current for $p = 0.9$ torr

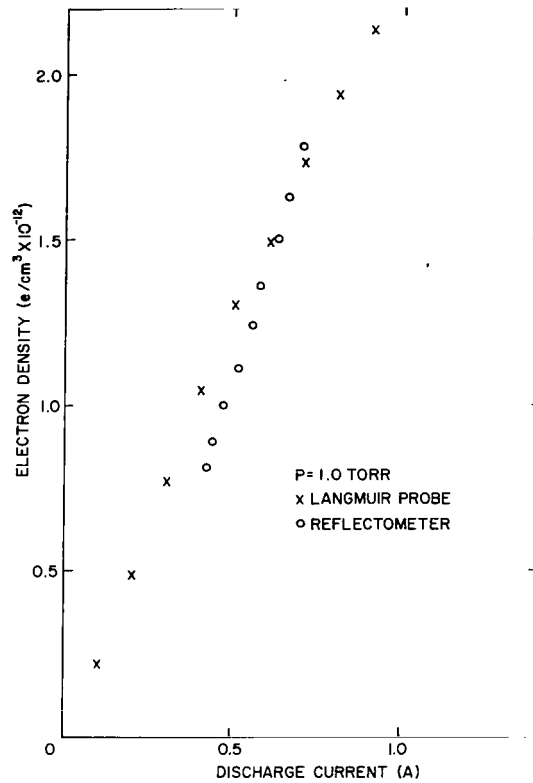


Figure 14.- Peak electron density as a function of discharge current for $p = 1.0$ torr

collisions are expected to be important (ref. 8). Hence, the total collision frequency is the combination of electron-neutral and electron-ion collision frequencies,

$$\nu_T = \nu_{en} + \nu_{ei} \quad (1)$$

The electron-neutral collision frequency is determined from published data on the collision cross-section for momentum transfer in helium (ref. 9) using

$$\nu_{en} = 100 \quad p P_C \sqrt{\frac{2kT_e}{m_e}} \quad (2)$$

where p is the pressure in torr, P_C is the collision probability in inverse cm at 1.0 torr, k is Boltzmann's constant, T_e is the electron temperature, and m_e is the electron mass. For the measured parameters of the discharge, the ratio ν_{en}/ω for a wave

frequency of 8.1 GHz ranges from about 0.003 to 0.007 for pressures between 0.4 and 1.0 torr. The following expression is used to calculate the electron-ion collision frequency (ref. 9);

$$\nu_{ei} = \left(\frac{2}{\pi}\right)^{\frac{1}{2}} \omega_p \frac{\ln(9n_D)}{9n_D} \quad (3)$$

where ω_p is the plasma frequency and n_D is the number of electrons in a Debye sphere. For electron densities corresponding to X-band cut-off frequencies and the temperatures of this experiment, this expression gives values larger than the electron neutral collision frequency by a factor of about 2 to 3, depending on the pressure. Of course, it is questionable whether Eq. (3) is accurate to this factor. In any event, it is expected that ν_{ei} is at least comparable to ν_{en} . Plots of ν_T/ω as a function of ω_p/ω for various pressures are shown in Figure 15.

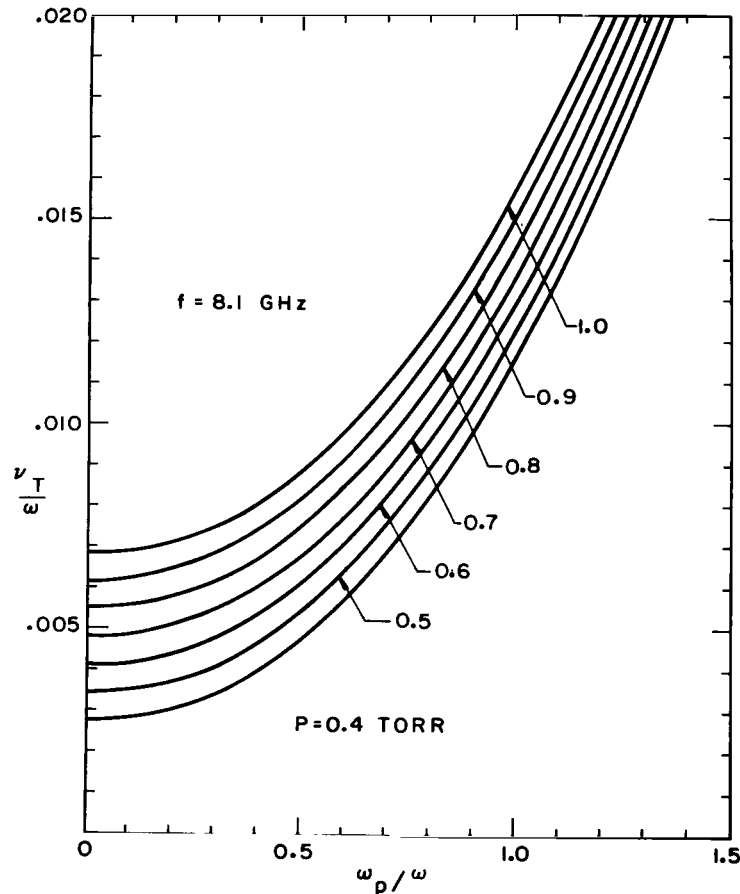


Figure 15. - The ratio of total collision frequency to wave frequency (8.1 GHz) as a function of normalized plasma frequency for various pressures

IV. THEORY OF PLASMA RADIATION

It is difficult to devise a theoretical model of radiation in the plasma just described which is tractable and is also a good approximation to the experimental situation. Some of the aspects of the experiment which are difficult to handle theoretically are: (1) the finite size of the anode and cathode; (2) the near field coupling of the antenna; (3) the spatial variation of the electron density and collision frequency;* and (4) the effects of antenna efficiency. In view of these difficulties, it was decided to study four theoretical models for comparison with the experimental data.

Model I

A high gain antenna, a uniform plasma slab bounded by free space, a constant collision frequency (spatially constant and independent of electron density), and incoherent reflections from both boundaries were assumed in Model I. The noise power emitted in such a case is well known and can be expressed as an equivalent temperature,

$$\frac{T_{eq}}{T_o} = \frac{\Gamma_p + (1 - 2\Gamma_p) e^{-\alpha d}}{1 - \Gamma_p e^{-\alpha d}} + \frac{(1 - \Gamma_p)(1 - e^{-\alpha d})}{1 - \Gamma_p e^{-\alpha d}} \frac{T_e}{T_o} \quad (4)$$

where T_o is the ambient temperature, T_e is the electron temperature, and

$$\Gamma_p = \left| \frac{\sqrt{\epsilon_p} - 1}{\sqrt{\epsilon_p} + 1} \right|^2 \quad \text{-power reflection coefficient}$$

$$\alpha d = 2D \left| \operatorname{Im} \sqrt{\epsilon_p} \right|$$

$$\epsilon_p = 1 - \frac{\omega_p^2}{\omega^2} (1 - j\frac{\nu}{\omega})^{-1}$$

$$D = \frac{\omega d}{c} \quad (5)$$

*The spatial variation of collision frequency is due to electron-ion collisions.

From the electron density profiles and radiometer frequency, D is expected to lie between 15 and 25. Figure 16 shows plots of the normalized equivalent temperature as a function of ω_p/ω for $D = 25$ and for various values of ν/ω .

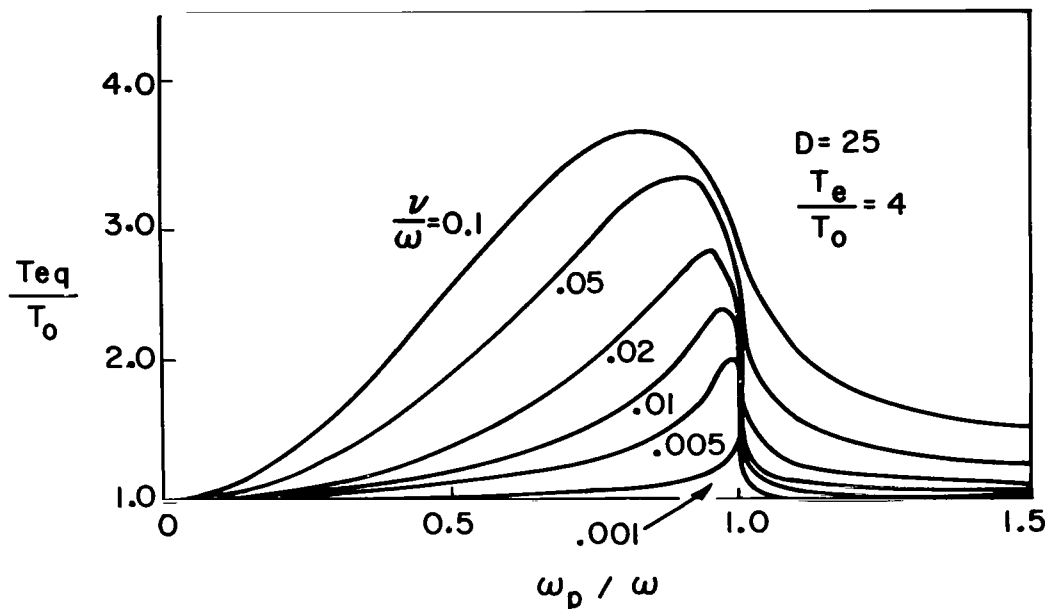


Figure 16. - Normalized equivalent plasma temperature based on Model I as a function of ω_p/ω for $D = 25$ and $T_e/T_0 = 4.0$

Model II

With collision frequencies comparable to the sum of $\nu_{en} + \nu_{ei}$ near $\omega_p = \omega$, Model II gives temperatures higher than the measured values for the reason that plasma reflections at both boundaries are assumed to contribute to the noise power received by the antenna. However, for a finite gain antenna, such as an open-ended waveguide, the boundary furthest from the antenna has little effect if d is many wavelengths. This is evident in the reflectometer results at zero plasma density where reflections from the aluminum cathode are negligible. Thus Model II is similar to Model I except that reflections from the boundary furthest from the antenna are neglected. Results using this model are shown in Figures 17 and 18

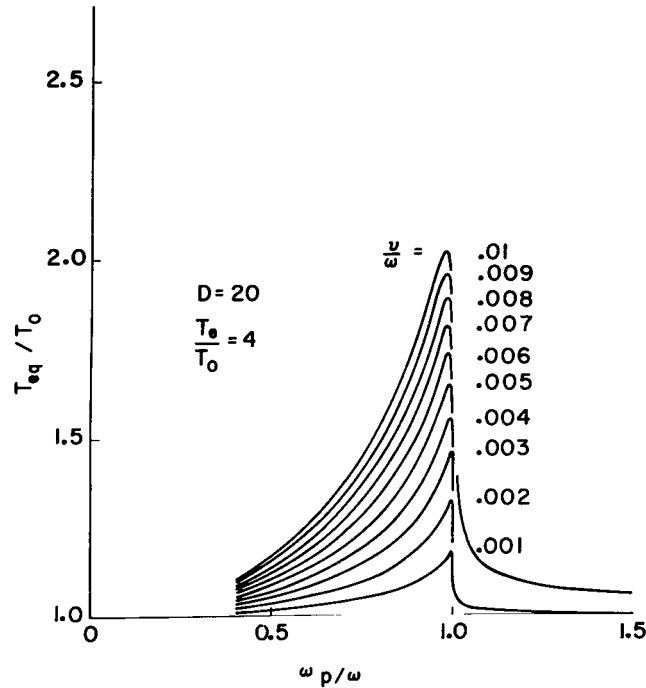


Figure 17. - Normalized equivalent plasma temperature based Model II as a function of ω_p/ω for $D = 20$ and $T_e/T_0 = 4.0$

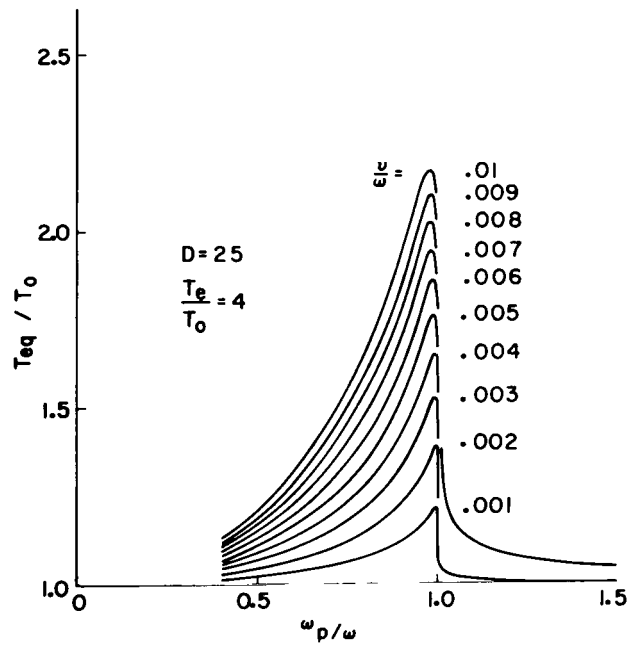


Figure 18. - Normalized equivalent plasma temperature based on Model II as a function of ω_p/ω for $D = 25$ and $T_e/T_0 = 4.0$

Model III

In Model III, the variation of ν_{ei} with ω_p/ω is included. Figure 19 shows the result of using Model II with the inclusion of both ν_{en} and ν_{ei} for $P = 0.4$ torr. Figure 20 shows a similar result with the electron-ion collision frequency reduced by a factor of 2. This arbitrary factor is consistent with the limits of validity of the expression yielding the electron-ion collision frequency. The term ν_{ei} is reduced by a factor of 2 for comparison with the experimental data, because these data will be shown to agree with the theory only if the collision frequency is lower than that given by Eq. (1). Also, the electron density profile which leads to a collision frequency profile should result in a lower effective collision frequency than that calculated on the basis of peak densities. This is especially true for the radiometer data where the major absorption, and hence reradiation, takes place near the antenna where the density is lower than the peak density. Comparing the results using this and the previous model indicates that the inclusion of electron-ion collisions changes the shape of the noise power curve, but obviously the peak power is described by the total collision frequency near $\omega_p = \omega$.

Model IV

In Model IV, the absorption coefficient of the plasma which, with the electron temperature, defines the plasma noise power, is calculated using a plane wave model (i.e., corresponding to a high-gain antenna); this includes the effects of electron density variations in the direction of propagation. For this case, the smoothed Langmuir probe data of Figures 4 through 14 are used, and profiles for currents between multiples of 0.1 A are obtained by interpolation. The number of computations are quite extensive, therefore, only one case is presented ($p = 0.4$ torr) in Figure 21. As expected, the peak noise power is higher than that of the uniform plasma slab theory.

In all four cases a ratio of electron temperature to ambient temperature of four is used ($T_e \approx 1200^\circ\text{K}$, $T_0 \approx 300^\circ\text{K}$). These results will be compared to the experimental data in Section V.

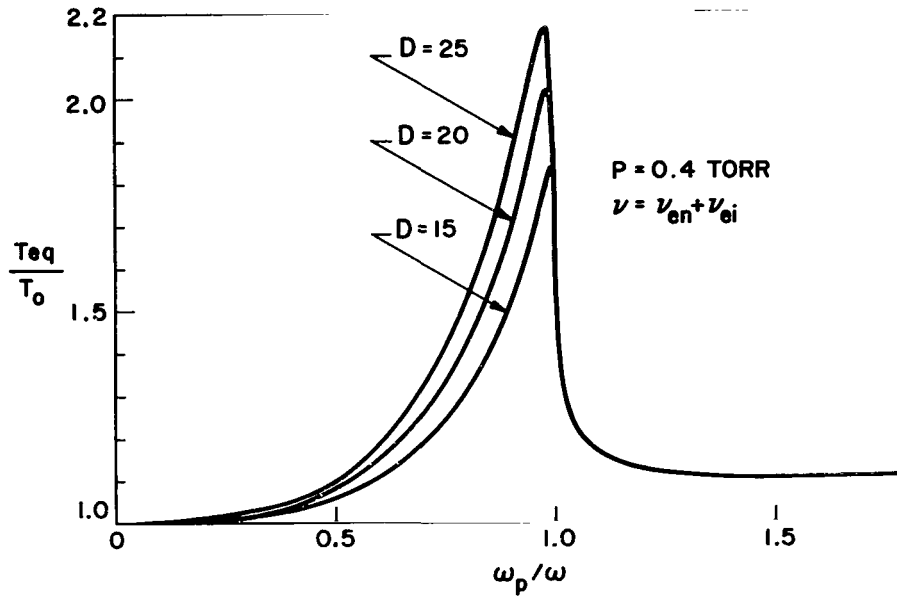


Figure 19. - Normalized equivalent plasma temperature, including electron-ion collisions, as a function of ω_p/ω for $p = 0.4$ torr

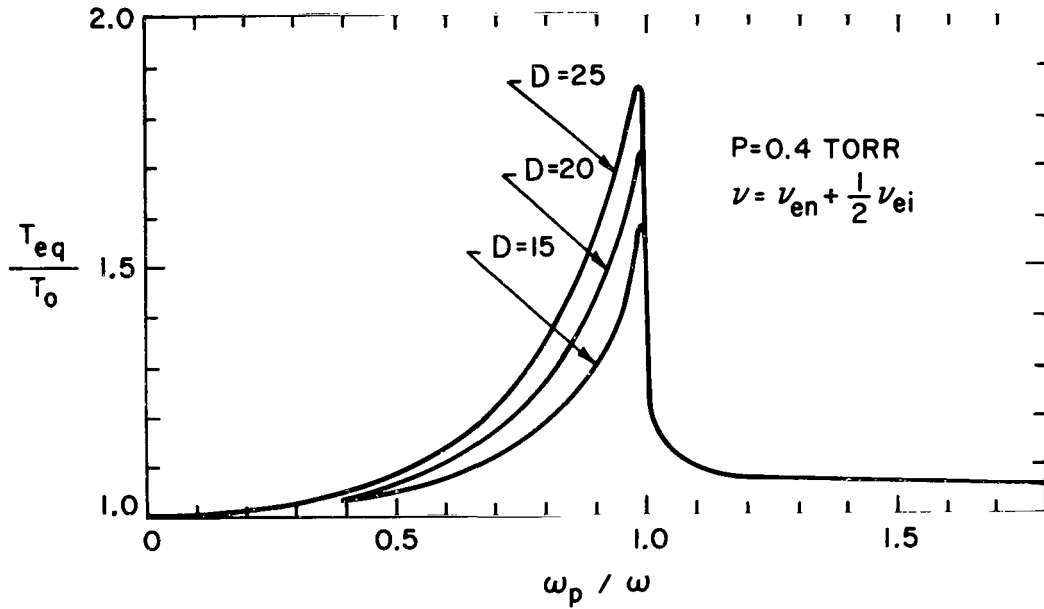


Figure 20. - Normalized equivalent plasma temperature as a function of ω_p/ω with the electron-ion collision frequency reduced by a factor of 2

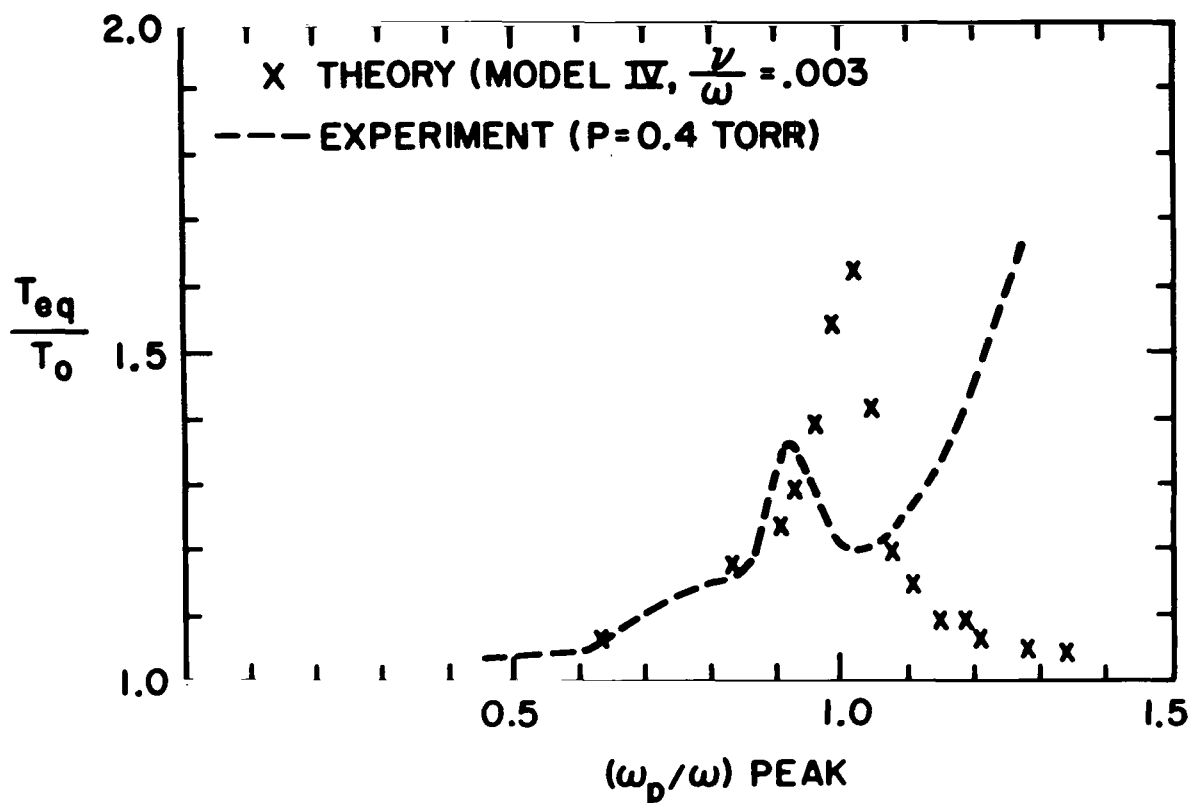


Figure 21. - Comparison of the experimental plasma noise data for $p = 0.4$ torr with the inhomogenous electron density, plane wave theory (Model IV)

V. PLASMA -- RADIOMETRIC INSTRUMENT CALIBRATION AND ANALYSIS

To obtain a precise measurement of the absolute temperature of a plasma at microwave frequencies, an antenna, the gain and efficiency of which is accurately known, and a radiometer capable of measuring signal power at the antenna output in units of equivalent absolute temperature are required. In addition, the RF transmission line between the plasma and the input signal port of a radiometer frequently compromise the capability of a radiometer to measure accurately a temperature because of the introduction of an added-circuit component which operates at different thermometric temperatures from the RF components of the radiometer system. However, a marked reduction in the effects of transmission line loss can be accomplished by operating the radiometric receiver in an "absolute temperature mode" (ref. 10) as explained in the appendix.

Prior to the measurement of the plasma temperature, a series of measurements of the antenna, associated transmission line, and RF components were conducted to determine the gain and efficiency

of the antenna as well as the insertion loss of the added transmission line and components between the radiometer and the plasma chamber. The efficiency of the antenna with no plasma reflections was measured by use of a calibrated absolute radiometer and a heated chamber lined with dark, absorbing material. The efficiency of the antenna was measured to be 80 percent. The insertion loss of the transmission line and the associated RF components was measured, and the value was determined to be less than .01 dB. Calibration of the radiometer for the absolute mode was accomplished by use of a known calibrated noise source which had a thermometric temperature of -77°K .

The accuracy obtained in the measurement of a plasma temperature at an equivalent absolute temperature T_a is determined by the accuracy to which the transmission line attenuation, directional coupler value, and the thermometric temperature of the individual passive components can be measured. The significance of these factors in determining the accuracy of an absolute temperature measurement of a plasma by use of a radiometer is best illustrated by the following parameters:

<u>Parameter</u>	<u>Value</u>
Instrument noise figure, F	7.5 dB
Receiver gain stability	1/100
Pre-detection bandwidth	10 MHz
Post-detection time constant	1 sec
Comparison load temperature	303°K
Thermometric temperature of passive components, T_L	303°K
Directional coupler value	9.85 dB
Transmission line loss	.01 dB
Radiometer sensitivity $^{\circ}\text{K rms } (\beta = 2)$	0.7°K
Output indicator fluctuation level, $^{\circ}\text{K}$	2.7
Antenna gain	17 dB
Antenna efficiency	80%
Accuracy of a single measurement, $^{\circ}\text{K}$	$\approx 1\%$
Amplitude of the calibration signal, $^{\circ}\text{K}$	15.6

VI. THE RADIOMETER DATA

An X-band radiometer, operating in an absolute temperature mode at a center frequency of 8.1 GHz, was used to measure noise power (expressed as an equivalent temperature) as a function of discharge current. The operating characteristics are described in the appendix. The radiometer was connected to the same open-ended waveguide used in obtaining the reflectometer results. The choice of an open-ended waveguide can be criticized, but it minimizes the plasma perturbation near the anode. If the need for a flush-mounted antenna in the immediate vicinity of the plasma is assumed*, the near field coupling is less than that for a higher gain antenna, such as a horn.

The discharge current was varied at a slow rate compared to the integration time of the radiometer, and the noise power as a function of discharge current for various pressures was recorded on a x-y recorder. For comparison of these data with the first three theoretical models, the current axis must be converted to the quantity ω_p/ω . The curves of peak density versus current obtained with the Langmuir probe are used for comparison purposes. The reduced data are shown in Figures 22 through 26. There is qualitative agreement between experiment and theory except for the rise in noise power for $\omega_p/\omega > 1$. As ω_p/ω increases from zero, the noise power increases due to plasma attenuation, peaks for ω_p/ω slightly less than 1, and decreases for $\omega_p/\omega \rightarrow 1$ due to plasma reflections. The subsequent rise is caused by the ground plane formed by the anode. In an infinite geometry, a perfectly conducting ground plane would eliminate the effects of plasma reflections, and no decrease in noise power would occur near $\omega_p/\omega = 1$. In the experiment, as ω_p/ω increases above 1, the effective plasma reflection point moves closer to the ground plane

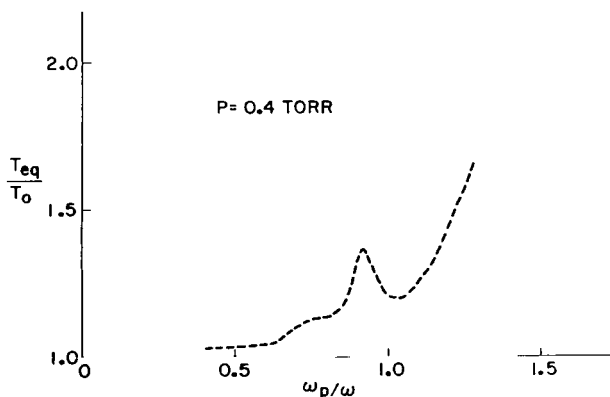


Figure 22.- Experimental plasma noise data for $p=0.4$ torr

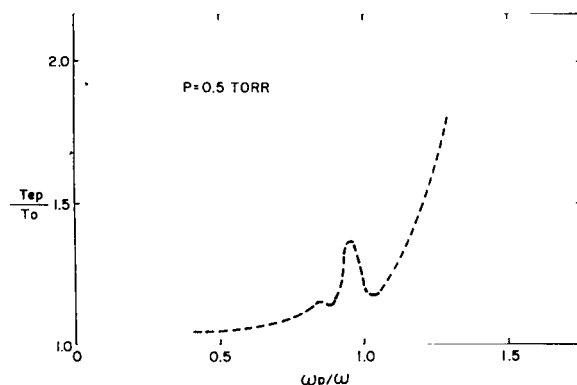


Figure 23.- Experimental plasma noise data for $p=0.5$ torr

*Typically a requirement for a re-entry measurement.

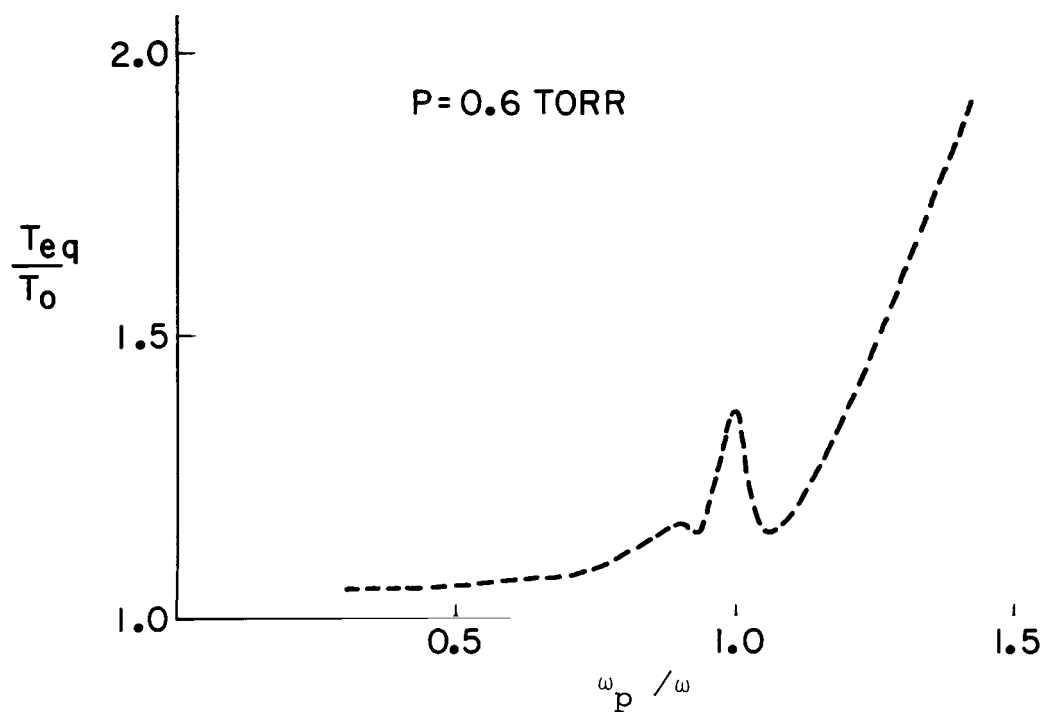


Figure 24. - Experimental plasma noise data for $p = 0.6$ torr

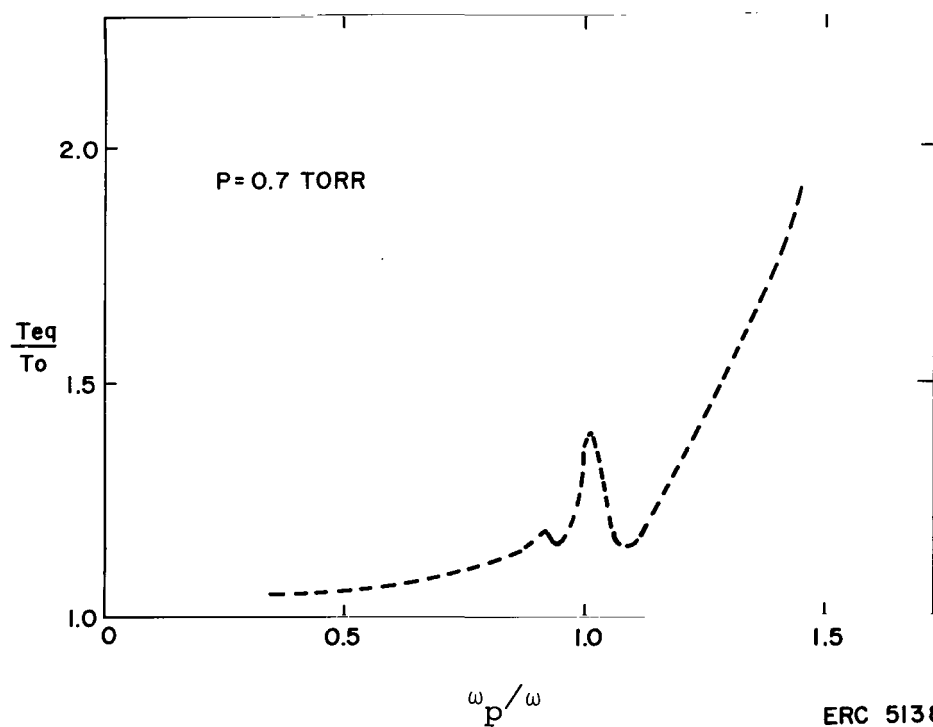


Figure 25. - Experimental plasma noise data for $p = 0.7$ torr

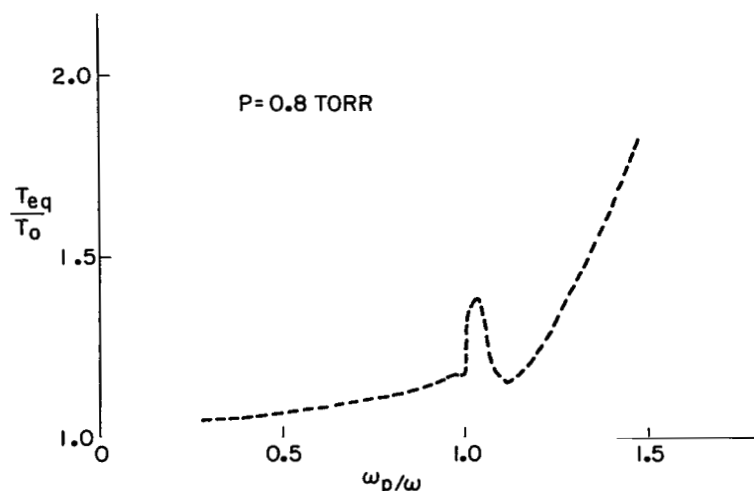


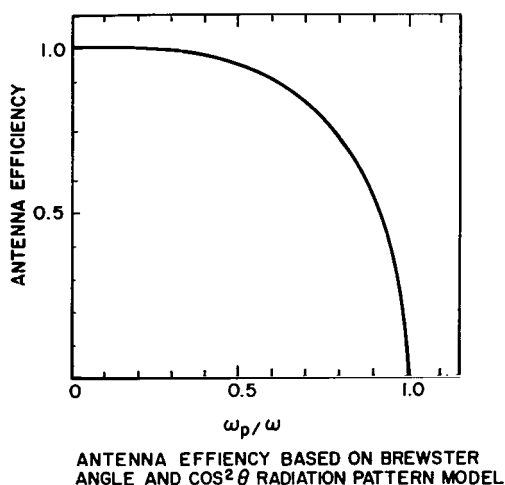
Figure 26. - Experimental plasma noise data for $p = 0.8$ torr

and the experiment approaches the infinite geometry, therefore, the noise power increases. This explanation was investigated by obtaining noise power data by use of an open-ended waveguide with no ground plane and with a radial direction of propagation. No increase in noise power for $\omega_p/\omega > 1$ was observed.

Some preliminary conclusions can be derived from attempts to fit the experimental data to the theoretical results. The shape of the noise power curves cannot be precisely matched by use of any of the four theoretical models. However, Model III would appear to give the best fit if the collision constants are suitably reduced. Figure 20 compares the experimental data for $p = 0.4$ with the results of Model IV. There is a difference in the location of the peak which is associated with the probe inaccuracy. The discrepancy in the magnitude of the peaks will be discussed later. Point by point matching is not shown for any of the first three models, since the authors feel that the shape of the curves is unduly influenced by factors not included in the theory. In particular, the shape is influenced by coherence effects between the first plasma interface and the ground plane due to the low collision frequency, and by the changes in electron density profile with current, which results in the effective plasma thickness and its location relative to the antenna being functions of discharge current. Therefore, it is not possible to obtain both electron temperature and collision frequency independently and accurately. Also, the measured peak power is lower than the peak power predicted by any of the four models when using the expected total collision frequency. Consequently, if the electron temperature is assumed to be known, the collision frequency, obtained from the peak noise power, is lower than

expected. One obvious explanation is the effect of antenna efficiency which is less than 100 percent and is a function of the plasma parameters. In view of the experimental difficulties cited in Section III, an exact calculation of the efficiency is not possible, and no tractable model appears to warrant detailed investigation. Therefore, as a crude indication of the effects of antenna efficiency, a hypothetical antenna with a $\cos^2 \theta$ power pattern is considered. Furthermore, the coupling to the plasma is assumed to be dictated by the reflection coefficient for angles less than the Brewster angle; otherwise zero coupling is assumed (ref. 11). Figure 27 shows the antenna efficiency as a function of ω_p/ω for this model. For the expected collision frequencies, the theory predicts that the peak noise power occurs for, $0.9 < \omega_p/\omega < 1$, and a crude estimate of antenna efficiency gives rather low values in this range.

In view of these conclusions, the electron temperature is assumed to be known, and the collision frequency is determined by matching the peak noise power obtained experimentally to the theoretical values when using Model II.* For low collision frequencies, the theoretical peak noise power is a single valued function of $(\nu/\omega) D$, and Figure 28 is a plot of these quantities for 100 and 50% antenna efficiencies. The peak, normalized equivalent temperature, obtained experimentally, lies in the



ERC 68-5312

Figure 27. - Antenna efficiency as a function of ω_p/ω

*As mentioned previously, Model III yields the best fit, but two collision constants must be adjusted and the better agreement is perhaps fortuitous.

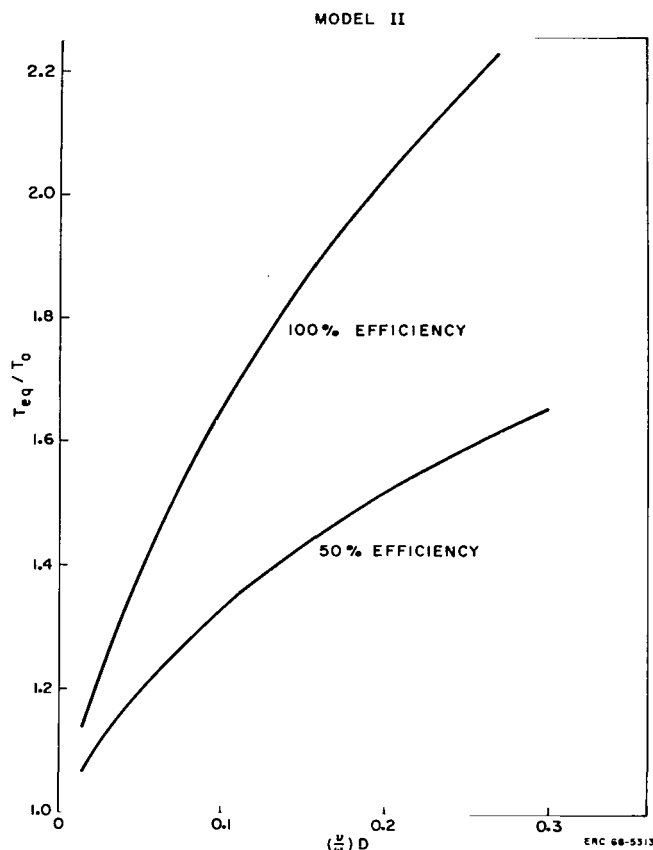


Figure 28. - The peak, equivalent, normalized plasma temperature as a function of $(\nu/\omega) D$ for two antenna efficiencies

vicinity of 1.35 to 1.4 which, if d is assumed to be 20, gives a ratio of collision frequency to wave frequency of between 0.003 and 0.007. This is a factor of 2 to 4 lower than expected. It is interesting to note that these experimental values are characteristic of ν_{en} alone. However, the experimental values do not vary appreciably with pressure and this indicates the importance of ν_{ei} .

VI.

VII. DISCUSSION OF REDIOMETRIC TECHNIQUE FOR RE-ENTRY FLIGHT MEASUREMENTS

Laboratory results have been presented showing how a curve of plasma noise power as a function of discharge current can be used to obtain the plasma parameters. The electron density is obtained from the location of the region of decreasing noise power subsequent to the peak power. The density is not precisely defined, but gives accuracy similar to a microwave reflectometer. In all the data presented here, the region of sharply decreasing noise power coincided with the region of increasing reflection coefficient of the microwave reflectometer operating at 8.1 GHz.

Because of the low electron temperature and low collision frequency of the laboratory plasma, it is not possible to obtain the electron temperature and collision frequency accurately and independently from the width and height of the noise power peak. However, when using the value of electron temperature obtained with the Langmuir probe, the measured collision frequency is found to be within at least a factor of 4 of the theoretical values; however, the collision theory is only good to a factor of 2 or 3. If the antenna efficiency is assumed to be 50 percent, the measured values are well within the theoretical accuracy.

In view of the laboratory results presented in this report, the microwave radiometer appears to be a promising device for measuring the re-entry plasmas of large, high-speed vehicles. In this case, the plasma temperature is high (5000 to 10,000°K); the collision frequency at low altitudes is typically less, but comparable to the plasma frequency; and the plasma is many free-space wavelengths thick for frequencies comparable to the plasma frequency. Figure 29 shows some theoretical curves (Model I) with plasma parameters characteristic of the plasmas of large, blunt, high-speed re-entry vehicles.

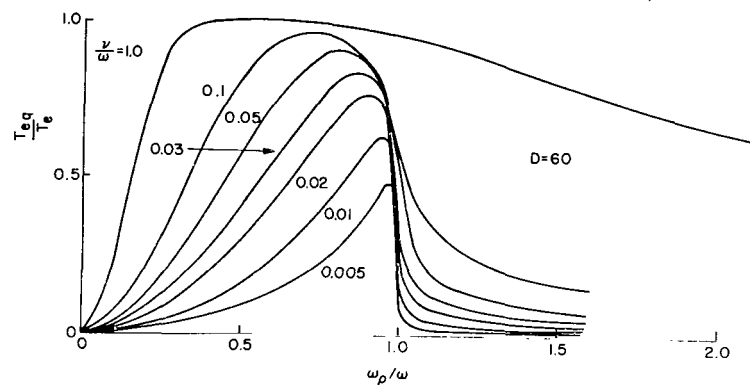


Figure 29. - Plasma noise as a function of ω_p/ω using Model I and parameters applicable to plasma of a large, blunt, high-speed vehicle

Under these conditions, the noise power peak is comparable to blackbody noise at the plasma temperature; the width of the curve is appreciable; and the antenna efficiency is higher. Hence, the three plasma parameters n_e , T_e , and v_T can be more accurately obtained. Of course, the re-entry measurement presents problems not encountered in the laboratory, such as the

presence of (1) a coating of ablation material; (2) plasma temperature profiles; (3) plasma turbulence. Also, the data must be obtained in a time interval which is short compared to the time for appreciable changes in the plasma parameters by using a swept-frequency radiometer or instantaneously by using several fixed-frequency devices.

Electronics Research Center
National Aeronautics and Space Administration
Cambridge, Massachusetts, March 1969
125-21-02-76

APPENDIX

ABSOLUTE RADIOMETRIC MODE

A simplified functional block diagram, showing the interconnection of RF components to achieve an absolute radiometric mode, is shown in Figure A-1. By appropriate adjustment of attenuator A, the output indicator zero corresponds to 0°K, and the indicator reads the effective noise power at the input signal port (1) of switch S directly in degrees Kelvin. The method of calibration and adjustment negates consideration of RF transmission line losses between the input signal port of switch S and the signal input port of the ferrite modulator M.

The method of calibration takes note of the fact that any noise power signal, presented to the input signal port of switch S, will be attenuated by the losses associated with the passive circuitry in the signal transmission from the signal input port of switch S to the input signal port of the modulator. Noise radiated by this passive circuitry will also be presented at the output signal ports of the modulator. The attenuation of the input signal can be characterized by a loss, L, and the effective temperature of the added noise by a bias temperature, T_b . If the effective temperature of the input signal noise power is T_s , the signal temperature at the input port of the modulator will be given by:

$$T_{IN} = \frac{T_s}{L} + T_b \quad (A-1)$$

Absolute temperature measurements usually involve techniques for determining the loss, L, through some form of a comparative attenuation measurement. The value of the radiated noise, T_b , is then deduced from its relationship to the measured value of L since:

$$T_b = (1 - \frac{1}{L}) T_L \quad (A-2)$$

where T_L is the thermometric temperature of the transmission line components which contribute to the loss, L. If the various parts of the RF circuit are not of the same temperature T_L , then a summation of various terms of the form (A-2) is required. If, however, all portions of the RF circuit preceding the modulator are maintained at a temperature T_α slightly above ambient, then the summation is not required, and (A-2) takes the form:

$$T_b = (1 - \frac{1}{L}) T_\alpha \quad (A-3)$$

The same argument follows for the transmission line from the dual reference oven control resistive loads at temperature T_α to comparison port (2) of the modulator. With switch S connected to port (2), the input power to either port of the modulator is then:

$$\frac{T_E}{L} + T_b = T_\alpha \quad (A-4)$$

Under this condition, the output indicator will be at a scale position of zero since the relative input power difference is zero at the modulator input ports.

Calibration of the instrument is accomplished by a single adjustment of attenuator A with a known source of noise power (cold load) at an effective temperature, T_K , connected to the signal input port of switch S. Under this condition, the effective signal temperature at input port (1) of the modulator will from prior reasoning be:

$$T_{IN} = \frac{T_K}{L} + T_b \quad (A-5)$$

Re-expressing the comparison temperature T_E in the form (A-4), the power difference between the modulator input ports can be written as:

$$\frac{T_K}{L} + T_b - \frac{T_\alpha}{L} - T_b = \frac{1}{L} (T_K - T_\alpha) \quad (A-6)$$

which provides a negative deflection at the output indicator proportional to the temperature difference between the environmental chamber, T_α , and the absolute temperature of the known source of noise, T_K . Though the proportionality factor is the reciprocal of the attenuation in the signal path transmission line, its measurement is not required. Calibration of the indicator scale in degrees Kelvin is obtained by noting that the measured negative deflection from the zero scale position is proportional to the temperature difference ($T_\alpha - T_K$).

With the noise generator ignited, attenuator A is then adjusted to provide an output indicator reading equivalent to the value of T_K , in the previously defined indicator scale units. The proportionality factor, $(1/L)$, is retained since the amount of noise injected into the signal path, referenced to modulator port (1), must be equal to $(T_\alpha - T_b)$. Only under this condition will the temperature difference between the two modulator parts take the form:

$$\left(\frac{T_K}{L} + T_b \right) + T_\alpha - T_b - T_\alpha = \frac{T_K}{L} \quad (A-7)$$

It is not necessary to know that the amount of injected noise required is $(T_{\alpha} - T_b)$, nor is it required that the value of T_b be known. The only requirement is that attenuator A be adjusted to provide an indicator reading corresponding to T_K , in the previously determined indicator units.

Verification of the calibration at any future time under operating conditions is obtained by connecting switch (S) in position (2) with the noise generator extinguished to provide a verification of the output indicator zero scale reading. Ignition of the noise generator will then provide a positive scale indication corresponding to an input signal noise temperature of T_{α} in the previously established relationship between indicator scale units and degrees Kelvin. The only adjustment that may be required at this time to provide the appropriate output indicator deflection is receiver gain. A constant of proportionality ($1/L$) will continue to influence the indicator reading but will not influence the absolute calibration of the output indicator scale.

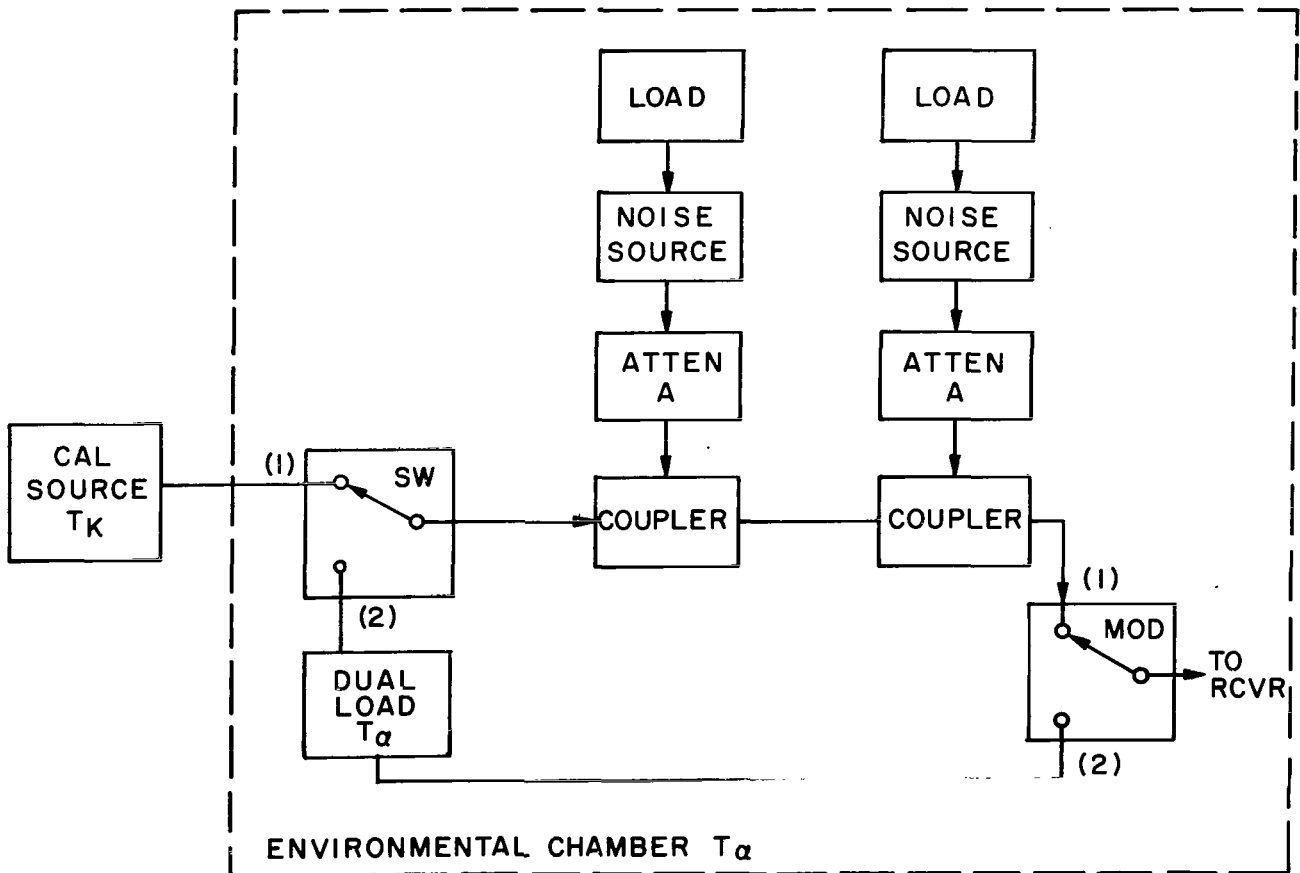


Figure A-1 - Simplified diagram of absolute radiometric mode

REFERENCES

1. Caldecott, R., Mayhan, J., and Bohley, P.: Antenna Noise Level and Impedance in a Re-entry Environment - Flight Test Results Using a Trailblazer Re-entry Vehicle and Some Related Laboratory Studies. Presented at Conference on the Applications of Plasma Studies to Re-entry Vehicle Communications, Wright-Patterson Air Force Base, Ohio, October 3-4, 1967.
2. Bekefi, G.: Radiation Processes in Plasmas. Wiley and Sons, 1966.
3. Ingraham, J. C.: Electron Relaxation Times in a Plasma. Ph.D. Thesis, M.I.T., Dept. of Physics (1967).
4. Kaminsky, M.: Atomic and Ionic Impact Phenomena on Metal Surfaces. Academic Press 1965, pp. 328-329.
5. Persson, K. B.: The Brush Cathode Plasma -- A Well Behaved Plasma. J. Appl. Phys., vol. 36, October 1965, pp. 3086-94.
6. Bates, D. R., and Delgarno, A.: Electronic Recombination. Atomic and Molecular Processes (edited by D. R. Bates), Academic Press, New York, 1962, pp. 245-271.
7. Crosswell, W. F., Taylor, W. C., Swift, C. T., and Cockrell, C. R.: The Input Admittance of a Rectangular Waveguide-Fed Aperture under an Inhomogenous Plasma: Theory and Experiment. IEEE Trans., vol. AP-16, no. 4., July 1968, pp. 475-487.
8. Bekefi, G.: Radiation Processes in Plasmas. Wiley and Sons, 1966, pp. 97-98.
9. Shkarofsky, I. P., Johnston, T. W., and Bachynski, M. P.: The Particle Kinetics of Plasmas. Addison-Wesley, 1966.
10. Haroules, G. G., and Brown, W. E.: Technique for Absolute Temperature Measurement at Microwave Frequencies. Rev. Sci. Inst., vol. 38, no. 8, August 1967, pp. 1093-1096.
11. Bachynski, M. P., and Cloutier, G. G.: Communications in the Presence of Plasma Media. RCA Res. Rpt. 7-801, 23 October 1962. Presented at the Symposium on Dynamics of Manned Lifting Planetary Entry, Philadelphia, Pa., October 29-31, 1962.

NATIONAL AERONAUTICS AND SPACE ADMINISTRATION
WASHINGTON, D. C. 20546
OFFICIAL BUSINESS

FIRST CLASS MAIL



POSTAGE AND FEES PAID
NATIONAL AERONAUTICS AND
SPACE ADMINISTRATION

NOV 19 1958
U.S. AIR FORCE
WASHINGTON, D.C. 20546

U.S. AIR FORCE
WASHINGTON, D.C. 20546

POSTMASTER: If Undeliverable (Section 158
Postal Manual) Do Not Return

"The aeronautical and space activities of the United States shall be conducted so as to contribute . . . to the expansion of human knowledge of phenomena in the atmosphere and space. The Administration shall provide for the widest practicable and appropriate dissemination of information concerning its activities and the results thereof."

— NATIONAL AERONAUTICS AND SPACE ACT OF 1958

NASA SCIENTIFIC AND TECHNICAL PUBLICATIONS

TECHNICAL REPORTS: Scientific and technical information considered important, complete, and a lasting contribution to existing knowledge.

TECHNICAL NOTES: Information less broad in scope but nevertheless of importance as a contribution to existing knowledge.

TECHNICAL MEMORANDUMS: Information receiving limited distribution because of preliminary data, security classification, or other reasons.

CONTRACTOR REPORTS: Scientific and technical information generated under a NASA contract or grant and considered an important contribution to existing knowledge.

TECHNICAL TRANSLATIONS: Information published in a foreign language considered to merit NASA distribution in English.

SPECIAL PUBLICATIONS: Information derived from or of value to NASA activities. Publications include conference proceedings, monographs, data compilations, handbooks, sourcebooks, and special bibliographies.

TECHNOLOGY UTILIZATION PUBLICATIONS: Information on technology used by NASA that may be of particular interest in commercial and other non-aerospace applications. Publications include Tech Briefs, Technology Utilization Reports and Notes, and Technology Surveys.

Details on the availability of these publications may be obtained from:

SCIENTIFIC AND TECHNICAL INFORMATION DIVISION
NATIONAL AERONAUTICS AND SPACE ADMINISTRATION
Washington, D.C. 20546